Journal of Materials Science: Materials in Electronics (2019) 30:5573–5579
https://doi.org/10.1007/s10854-019-00851-x

Electrode properties of a spinel family, AFe_2O_4 (A = Co, Ni, Cu), as new cathode for solid oxide fuel cells

Jinghao Cui[1] · Yuhan Gong[1] · Runze Shao[1] · Shaoshuai Wang[1] · Jialun Mao[1] · Meng Yang[1] · Weifeng Wang[1] · Qingjun Zhou[1]

Received: 4 October 2018 / Accepted: 29 January 2019 / Published online: 11 February 2019

Abstract
In this work, the spinel-type oxides of AFe_2O_4 (A = Co, Ni, Cu) prepared via a glycine–nitrate process were investigated as possible cathode materials for solid oxide fuel cells. The as prepared sample, $CoFe_2O_4$ and $NiFe_2O_4$ are cubic spinel structure, while the $CuFe_2O_4$ is tetragonal spinel structure. The XRD results show that AFe_2O_4 (A = Co, Ni, Cu) is chemically compatible with $La_{0.9}Sr_{0.1}Ga_{0.8}Mg_{0.2}O_{3-\delta}$ (LSGM) at fuel cell operation temperatures. At a given temperature, the order of the electrical conductivity of the ceramic samples was $CuFe_2O_4 > CoFe_2O_4 > NiFe_2O_4$. The electrical conductivity of $CuFe_2O_4$ reaches a maximum value of 2.7 S cm^{-1} at 850 °C in air. The order of average thermal expansion coefficient was $CuFe_2O_4 < NiFe_2O_4 < CoFe_2O_4$ in the temperature range of 30–1000 °C in air. The thermal expansion coefficients of the AFe_2O_4 (A = Co, Ni, Cu) samples are very close to that of typical electrolyte materials. $CuFe_2O_4$ exhibits the smallest area specific resistance among the three samples, i.e., 0.37 Ω cm^2 at 800 °C in air. Peak power density of single cells with $CuFe_2O_4$ as cathode on a 300 μm-thick LSGM electrolyte reaches 326 mW cm^{-2} at 800 °C. In this series, $CuFe_2O_4$ exhibits a favorable oxygen reduction reaction activity, thus it may be a promising candidate in SOFCs.

1 Introduction

In the last few years, great efforts have been devoted to extending the lifespan and reducing the fabrication cost of solid oxide fuel cells (SOFCs). Consequently, exploring SOFCs operating at intermediate- or low-temperature has become one of the most popular and urgent topics [1–15]. A typical SOFC is composed of a porous anode, a dense electrolyte film, and a porous cathode. Generally, SOFC, the cathode provides the reaction site where oxygen molecules are reduced to oxygen ions (½ O_2 (g) + $2e^- \rightarrow O^{2-}$) within a SOFC structure. Recently, cobalt-containing perovskites have been extensively studied as potential cathodes of SOFCs because of their high oxygen reduction reaction activity (ORR) catalytic activity, such as $Ln_{1-x}Sr_xCo_{1-y}Fe_yO_{3-\delta}$ (Ln = rare-earth) [2, 16, 17], $Ba_{1-x}Sr_xCo_{1-y}Fe_yO_{3-\delta}$ [1, 18] and $LnBaCo_2O_{5+\delta}$ (Ln = rare-earth) [4, 19]. However, the limitations of these cobalt-containing perovskite have hindered their further applications, such as the high cost of rare earth elements, large thermal expansion coefficient (TEC) values, Cr poisoning from the interconnects and poor chemical stability where the alkaline earth metals in the cathode is subject to react with CO_2 to form carbonates [20–24]. Therefore, it is extremely necessary to develop effective cathode materials for SOFCs with good TEC compatibility with adjacent components, high electrocatalytic activity and stability.

Most recently, spinel oxides have become attractive structures as alternative cathode materials for SOFCs, demonstrating good thermal expansion compatibility with electrolytes, superior electrochemical performance, high thermal and chemical stability. The spinel oxides were first studied as protective layers coated on ferric stainless steel interconnects to prevent Cr diffusion from the interconnect to the cathode, where Cr diffusion greatly degrades the catalytic activity of the cathode material for ORR [25–31]. Recently, several spinel-type metal oxides have attracted attentions as alternative cathode materials for SOFCs [32–38]. As spinel oxides are rare-earth or alkaline-earth free, they rarely react with the adjacent components of SOFCs to form high resistance phases, compared with the traditional perovskite cathodes. Therefore, the chemical compatibility is good between the spinel cathode and other adjacent components. However, the

✉ Qingjun Zhou
qjzhousofc@163.com; qjzhou@cauc.edu.cn

[1] College of Science, Civil Aviation University of China, Tianjin 300300, People's Republic of China

activity of spinel cathode is not satisfactory so that the electrochemical performance requires to be further improved. Rao et al. reported the spinel cathode $NiFe_{1.5}Co_{0.5}O_4$ shows good electrochemical performance with a polarization resistance value of 0.73 Ω cm^2 at 700 °C and a maximum power density of 320 mW cm^{-2} at 600 °C with a 38-μm-thick SDC electrolyte [34]. Shao et al. reported the spinel cathode $CuCo_2O_4$ displays a polarization resistance of 0.12 Ω cm^2 at 800 °C and a maximum power density of 972 mW cm^{-2} at 800 °C with a 10-μm-thick SSZ electrolyte [36].

In this article, spinel-type oxides with nominal composition of AFe_2O_4 (A = Co, Ni, Cu) has been synthesized and systematically studied concerning their structure, chemical compatibility, electrical conductivity, thermal expansion behavior, and electrochemical performance towards ORR as new cathode materials for SOFCs.

2 Experimental

2.1 Sample synthesis and cell fabrication

AFe_2O_4 (A = Co, Ni, Cu) powders were prepared using a glycine–nitrate process. To synthesize the AFe_2O_4 (A = Co, Ni, Cu) powders, stoichiometric amounts of $Co(NO_3)_2{\cdot}6H_2O$, $Ni(NO_3)_2{\cdot}6H_2O$, $Cu(NO_3)_2{\cdot}3H_2O$ and $Fe(NO_3)_3{\cdot}9H_2O$ were dissolved in deionized water. Glycine was then added as the fuel and complexant. The mixed solution was subsequently stirred and heated slowly to obtain a transparent gel, and ignited to flame, with a black ash remaining. Finally, the ash was collected and calcined at 900 °C for 5 h to form a spinel phase.

For symmetric cell and single fuel cell measurement purposes, LSGM, $Ce_{0.8}Sm_{0.2}O_{1.9}$ (SDC), and NiO powders were also synthesized by the glycine–nitrate process as previously described [39, 40]. The anode powder, composed of 65 wt% NiO and 35 wt% SDC, was well mixed in liquid ethanol by ball-milling treatment for 5 h. The fabrication procedures for the LSGM electrolyte supported symmetrical cells and single fuel cells is described elsewhere [41, 42]. Symmetrical (single) cells with $CoFe_2O_4$, $NiFe_2O_4$ and $CuFe_2O_4$ spinel cathodes were then calcined at 1000 °C for 2 h in air with an effective electrode area of 0.25 cm^2, respectively. The single fuel cell was sealed onto one end of an alumina tube by silver paste.

2.2 Characterization and electrochemical measurements

The phase purity and chemical compatibility of the as-prepared AFe_2O_4 (A = Co, Ni, Cu) powders were characterized by X-ray diffraction (XRD) (Rigaku-D-Max Ra system) with an angle step of 0.02° and a scanning range of 20°–80° at room temperature. Electrical conductivity was measured by van der Pauw method from 600 to 850 °C at intervals of 50 °C in air. The TEC of the samples were measured using a dilatometer (Netsch DIL 402 Expedis Classic) in air from 30 to 1000 °C, with an air-purge flow rate of 60 mL min^{-1} and a heating rate of 5 °C min^{-1}. The electrochemical impedance spectra (EIS) was recorded using an electrochemical workstation (Zaher Im6ex), and the impedance frequency was set from 1 MHz to 0.1 Hz with an excitation potential of 10 mV at the temperature range of 700–800 °C at an interval of 50 °C. Samples were tested under an open circuit voltage (OCV) condition in air. The single-cell performance was tested from 650 to 800 °C by an electrochemical analyzer (Ivium Technologies) with humidified hydrogen (flow rate: 50 mL min^{-1}) and ambient air supplied as the fuel and the oxidant, respectively. A stabilization time of 30 min was allowed for each testing point. The microstructure of the cell after testing were observed using a Nova NanoSEM230 field emission scanning electron microscope (FE-SEM, FEI, the Netherlands).

3 Result and discussion

3.1 Phase and chemical compatibility characteristics

Figure 1 shows the room temperature XRD patterns of AFe_2O_4 (A = Co, Ni, Cu) powders after calcining at 900 °C for 5 h in air. As shown in Fig. 1, $CoFe_2O_4$ and $NiFe_2O_4$ exhibit a cubic spinel structure that belongs to the Fd-3m (227) space group with no impurities found. $CuFe_2O_4$ has a tetragonal structure with a space group of I41/amd (141),

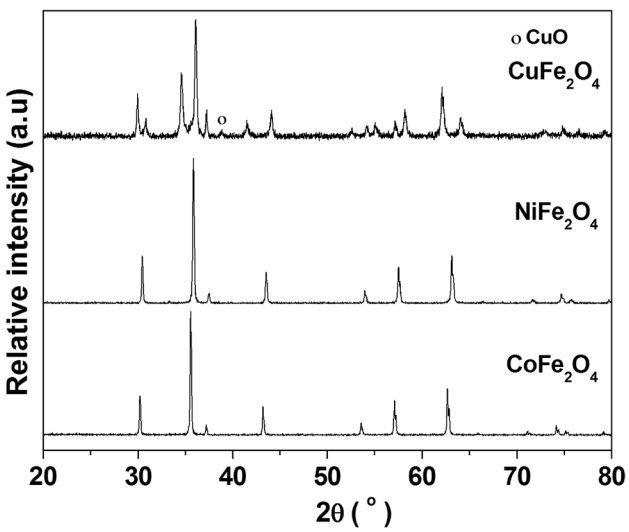

Fig. 1 XRD patterns of AFe_2O_4 (A = Co, Ni, Cu) powders after sintering at 900 °C for 5 h

but it contains small quantities of CuO impurity phase. To examine the chemical compatibility between the AFe_2O_4 (A = Co, Ni, Cu) cathode materials and the LSGM electrolytes, mixtures of the powders in a 1:1 weight ratio (cathode:electrolyte) were calcined at 1000 °C for 5 h in air. Figure 2a–c shows that there are no extra peaks observed for the mixed powders, indicating that no chemical interactions and/or inter-diffusion of elements occurred between the cathodes and the electrolytes at 1000 °C. This result indicates that AFe_2O_4 (A = Co, Ni, Cu) cathodes have good chemical compatibility with the LSGM electrolyte under fuel cell fabrication conditions.

3.2 Electrical conductivity

The total electrical conductivity of AFe_2O_4 (A = Co, Ni, Cu) ceramics was measured in the temperature range 600–850 °C in air. As depicted in Fig. 3a, AFe_2O_4 (A = Co, Ni, Cu) oxides show gradually increasing electrical conductivity with increasing the temperature, exhibiting a semiconducting behavior in the whole studied temperature range. At a given temperature, $CuFe_2O_4$ shows the highest conductivity in this series, the order of the electrical conductivity follow the rule of $CuFe_2O_4 > CoFe_2O_4 > NiFe_2O_4$. For example, values of the electrical conductivities are 2.7, 0.69 and 0.12 S cm^{-1} for $CuFe_2O_4$, $CoFe_2O_4$ and $NiFe_2O_4$, respectively, at 850 °C in air. The largest electrical conductivity of $CuFe_2O_4$ among the three materials investigated could be attributed to the presence of Cu^+ and Cu^{2+} ions on the octahedral sites, thus increasing the electrical conductivity [43].

As shown in Fig. 3b, the linear relationship of Ln(σT) with 1/T can be observed in the whole temperature range studied, suggesting a small-polaron conducting mechanism, following the formula (1):

$$\sigma = \left(\frac{A}{T}\right) \times \exp\left(-\frac{E_a}{kT}\right) \quad (1)$$

where A is a material constant parameter, T is the absolute temperature, k is the Boltzmann constant and Ea is the activation energy. Here, the E_a values, which were calculated from the slope of the Arrhenius plot, are 0.69, 0.98 and 1.03 eV for $CuFe_2O_4$, $CoFe_2O_4$ and $NiFe_2O_4$, respectively.

3.3 Thermal expansion behavior

A good thermal-expansion compatibility between cathode and electrolyte leads to better structural stability in long-term operation and during thermal cycling of SOFCs. Figure 4 displays the thermal expansion behavior of AFe_2O_4 (A = Co, Ni, Cu) oxides between 30 and 1000 °C in air. The calculated TECs for four different temperature ranges are listed in Table 1. The average TECs in the range of 30−1000 °C

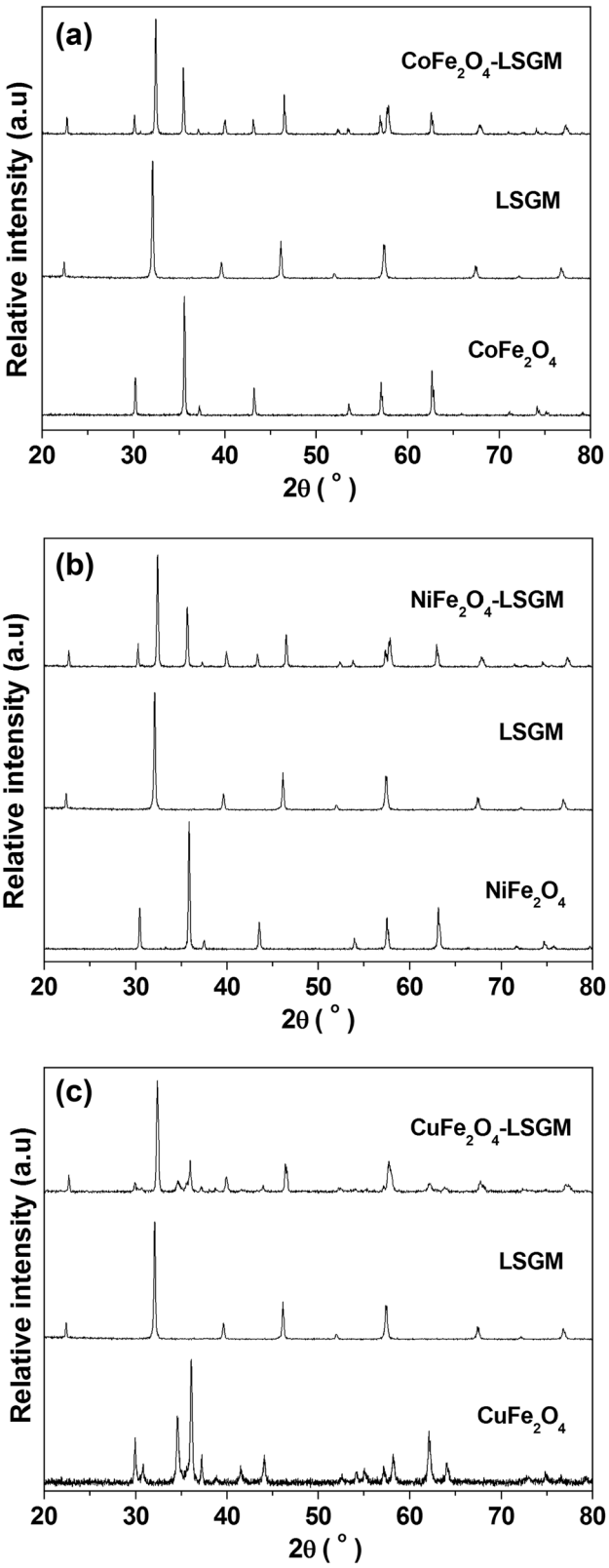

Fig. 2 XRD patterns of AFe_2O_4 (A = Co, Ni, Cu) and LSGM mixtures fired at 1000 °C for 5 h in air: **a** $CoFe_2O_4$–LSGM mixtures, **b** $NiFe_2O_4$–LSGM mixtures, **c** $CuFe_2O_4$–LSGM mixtures

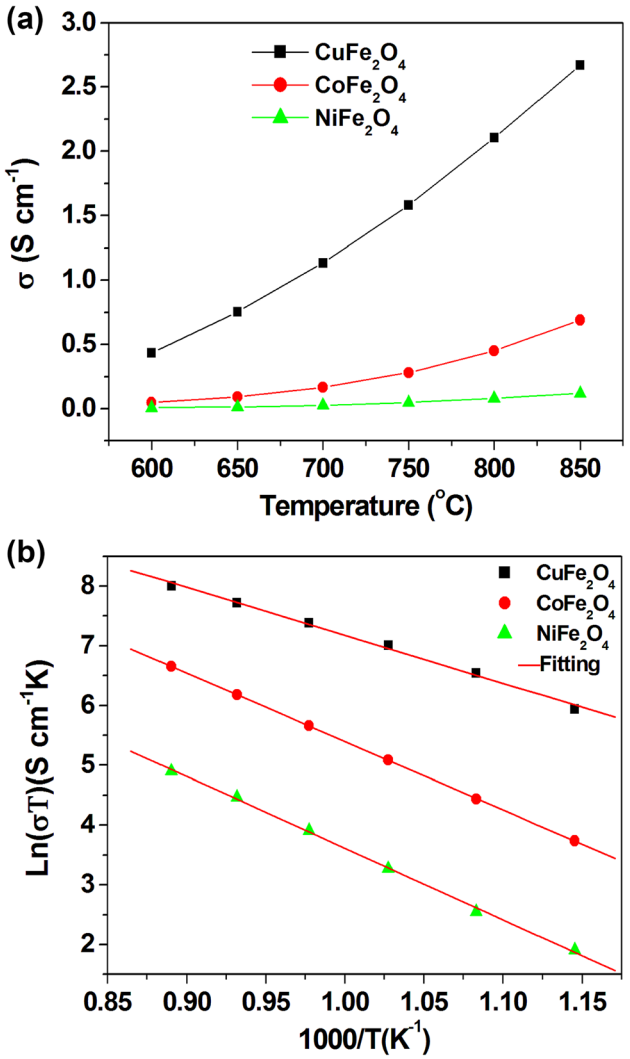

Fig. 3 Temperature dependence of the conductivity for AFe_2O_4 (A = Co, Ni, Cu) materials in air

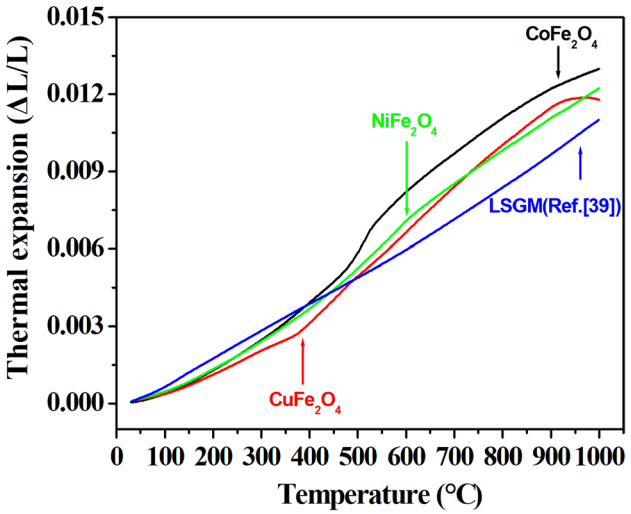

Fig. 4 Thermal expansion curves of AFe_2O_4 (A = Co, Ni, Cu) and LSGM [39] in the temperature range of 30–1000 °C in air

Table 1 The TECs value of AFe_2O_4 samples within specific temperature ranges

Temperature (°C)	TEC ($\times 10^{-6}$ K^{-1})		
	$CoFe_2O_4$	$NiFe_2O_4$	$CuFe_2O_4$
30–350	9.7	9.3	7.5
350–550	20.6	15.5	16.4
550–1000	12.7	13.6	13.4
30–1000	13.4	12.5	12.1

are 13.4×10^{-6} K^{-1}, 12.5×10^{-6} K^{-1} and 12.1×10^{-6} K^{-1} for $CoFe_2O_4$, $NiFe_2O_4$ and $CuFe_2O_4$, respectively, close to that of LSGM (11.3×10^{-6} K^{-1}) electrolyte [39]. These values are comparable with the results as reported in ref. $Cu_{1.4}Mn_{1.6}O_4$ (12.1×10^{-6} K^{-1} [37]) and $CuCo_2O_4$ (11.76×10^{-6} K^{-1} [36]) spinel cathodes, and are much lower than those of other cobalt-based (or cobalt-free) perovskite cathodes, such as $BaBi_{0.05}Co_{0.8}Ta_{0.15}O_{3-\delta}$ (20×10^{-6} K^{-1} [44]), $SmBaCo_2O_{5+x}$ (19.1×10^{-6} K^{-1} [20]), $Ba_{0.95}La_{0.05}FeO_{3-\delta}$ (24.5×10^{-6} K^{-1} [45]) and $Sm_{1.875}Ba_{3.125}Fe_5O_{15-\delta}$ (17.2×10^{-6} K^{-1} [46]).

3.4 Electrochemical performance

The ORR activity of the AFe_2O_4 (A = Co, Ni, Cu) system was analyzed by AC impedance spectroscopy based on a symmetric cell with the configuration of cathode/electrolyte/cathode. Figure 5a–c show typical impedance spectra for $CoFe_2O_4$/LSGM, $NiFe_2O_4$/LSGM and $CuFe_2O_4$/LSGM interfaces under OCV conditions. The difference between the real axis intercepts of the impedance plot is the area specific resistance (ASR). For comparison, the variation of ASR values with temperature for AFe_2O_4 (A = Co, Ni, Cu) samples is given in Table 2. The ASR values significantly decrease with increasing temperature for the same sample. An ASR of only 0.37 Ω cm^2 was obtained for the $CuFe_2O_4$ cathode at 800 °C, which is comparable to that of cells with the $Mn_{1.5}Co_{1.5}O_4$ cathode at the same temperature (0.43 Ω cm^2) [35]. $CuFe_2O_4$ exhibits the smallest ASR among three samples investigated. For instance, ASR for the $CoFe_2O_4$, $NiFe_2O_4$ and $CuFe_2O_4$ in air are 1.45, 1.56, and 0.37 Ω cm^2 at 800 °C, respectively. In addition, the ASR values of the $CoFe_2O_4$ and $NiFe_2O_4$ are similar in the temperature range studied. The sluggish performance of the $CoFe_2O_4$ and $NiFe_2O_4$ cathodes could be probably ascribed to their significantly low electronic and ionic conductivities [34].

In addition, the performance of AFe_2O_4 (A = Co, Ni, Cu) for ORR is further evaluated in single fuel cell under practical operating conditions. Figure 6 shows the performance

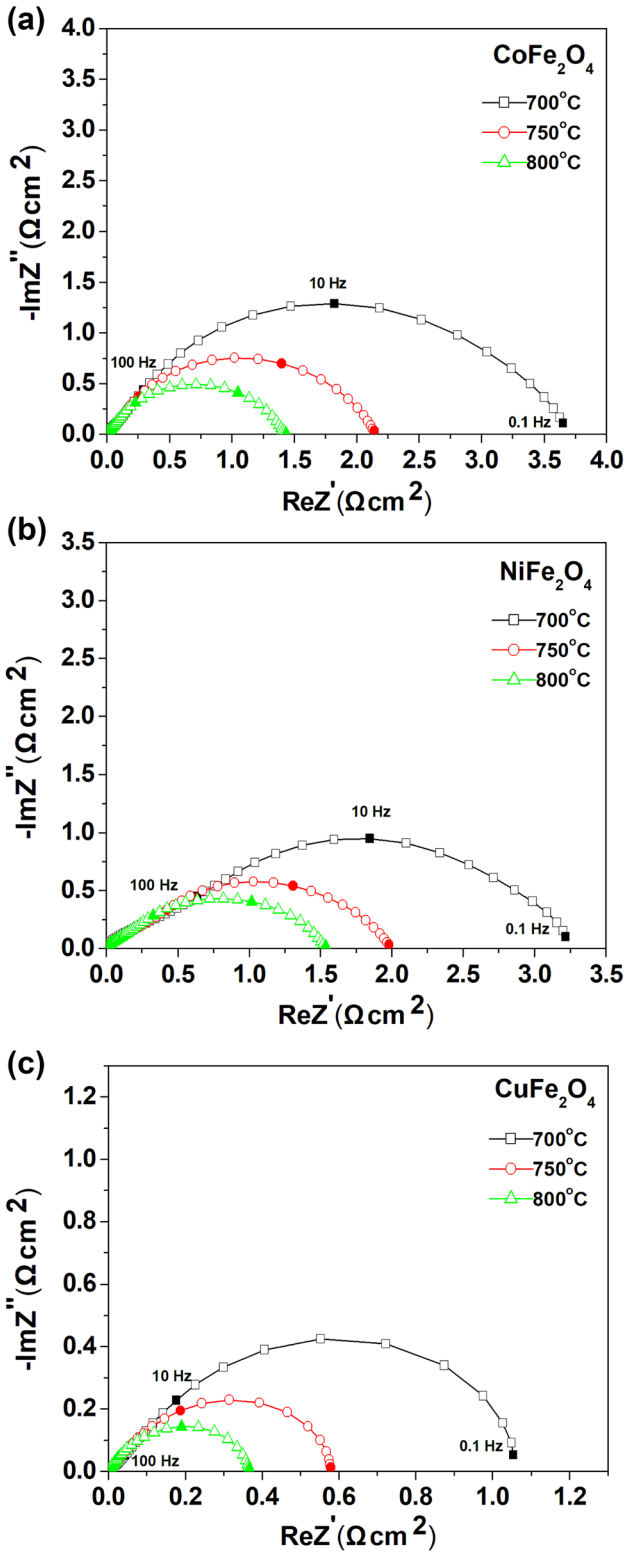

Fig. 5 Nyquist plots of AFe_2O_4/LSGM/AFe_2O_4 symmetric cells at 700–800 °C in air under open circuit conditions. For comparison, the ohmic resistance was subtracted from the experimental data

Table 2 ASR values of AFe_2O_4 cathode on LSGM electrolytes

Samples	Temperature (°C)		
	700 °C	750 °C	800 °C
$CoFe_2O_4$ (Ω cm^2)	3.71	2.17	1.45
$NiFe_2O_4$ (Ω cm^2)	3.27	2.02	1.56
$CuFe_2O_4$ (Ω cm^2)	1.06	0.58	0.37

of a LSGM electrolyte supported single fuel cell with the configuration of NiO–SDC/SDC/LSGM/AFe_2O_4 tested with pure hydrogen as a fuel and ambient air as an oxidant in the temperature range of 650–800 °C. SDC interlayer was applied between the anode (NiO–SDC) and electrolyte (LSGM) to avoid chemical interaction between LSGM and NiO. The thickness of the LSGM electrolyte is about 300 µm. Figure 6a–c show the I–V and I–P curves of the single SOFCs recorded from 650 to 800 °C. As expected, the single-cell with $CuFe_2O_4$ cathode exhibits the highest power densities compared to those with $CoFe_2O_4$ and $NiFe_2O_4$ cathodes. The peak power densities of single-cell with $CuFe_2O_4$, $CoFe_2O_4$ and $NiFe_2O_4$ cathodes are 326, 293 and 277 mW cm^{-2} at 800 °C, respectively. This result is in good agreement with the results of the electrical conductivity and the ASR results mentioned above. Such results are considered to be attractive when considering the 300 µm thickness of electrolyte. The cell performance can be further improved by decreasing the thickness of the electrolyte and optimizing the microstructure of the cathode.

In order to further investigate the thermal compatibility between the $CuFe_2O_4$ cathode and the LSGM electrolyte, SEM micrograph of the cross-sectional view of the half cell after testing was shown in Fig. 7. It can be seen that $CuFe_2O_4$ and LSGM have a good bonding and continuous contact at the interface, suggesting a good thermal compatibility between the cathode and electrolyte components, in agreement with the results of the TEC measurement.

4 Conclusions

The AFe_2O_4 (A = Co, Ni, Cu) has been prepared successfully using glycine–nitrate process. All these three oxides are of typical spinel structures. The AFe_2O_4 (A = Co, Ni, Cu) cathodes demonstrate good chemical compatibility with the LSGM electrolyte at the temperatures up to 1000 °C. AFe_2O_4 (A = Co, Ni, Cu) oxides show gradually increasing electrical conductivity with increasing temperature, exhibiting a semiconducting behavior in the whole temperature range investigated. These oxides show a good thermal expansion coefficient, close to that of the typical electrolyte materials. Among the AFe_2O_4 series, $CuFe_2O_4$ shows the best electrochemical performance. The ASR of AFe_2O_4 (A = Co,

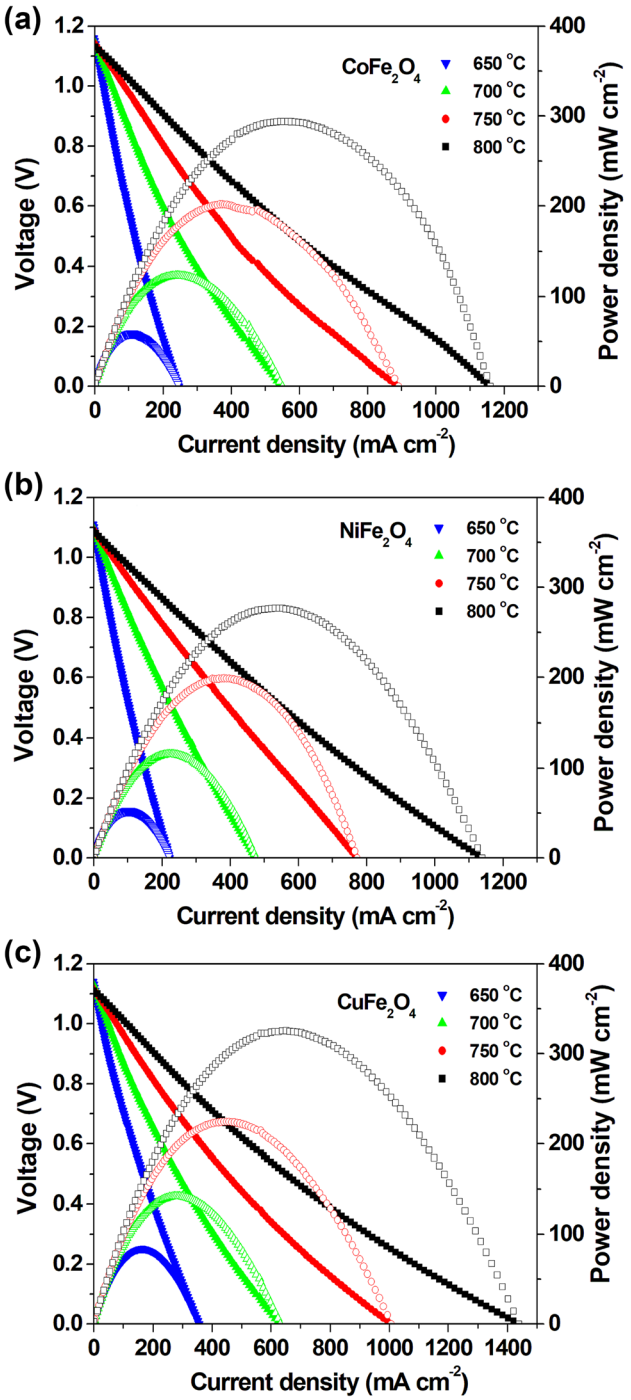

Fig. 6 Voltage and power density as a function of current density for an Ni–SDC/SDC/LSGM/AFe_2O_4 cell using H_2 as fuel and air as oxidant between 650 and 800 °C

Ni, Cu) symmetrical cells is 1.45 Ω cm^2, 1.56 Ω cm^2, and 0.37 Ω cm^2 respectively, at 800 °C. The electrolyte supported cells with the configuration of NiO–SDC/SDC/LSGM/AFe_2O_4 (A = Co, Ni, Cu) show peak power density of 293, 277, and 326 mW cm^{-2} at 800 °C, respectively. In spite the catalytic activity of AFe_2O_4 (A = Co, Ni, Cu) still

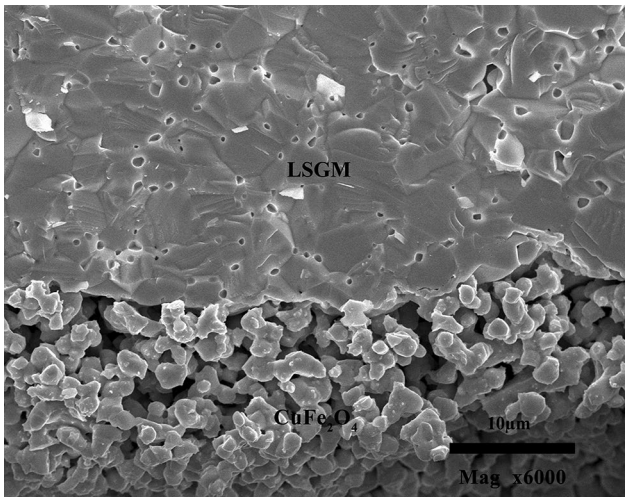

Fig. 7 SEM images of cross-sectional views of the LSGM/$CuFe_2O_4$ after testing

deserves further investigation in details, considering the overall performance, it is suggested that $CuFe_2O_4$ is an optimum cathode material for SOFCs.

Acknowledgements The research was financially supported by the National Undergraduate Training Programs for Innovation and Entrepreneurship (Grant No. IECAUC2017027), Fundamental Research Funds for the Central Universities (Grant No. 3122017083) and Scientific Research Project of Tianjin Education Committee (Grant No. 2018KJ254).

References

1. Z.P. Shao, S.M. Haile, Nature **431**, 170–173 (2004)
2. C.R. Xia, W. Rauch, F.L. Chen, M.L. Liu, Solid State Ion. **149**, 11–19 (2002)
3. L.D. Fan, B. Zhu, P.C. Su, C.X. He, Nano Energy **45**, 148–176 (2018)
4. Q.J. Zhou, T.M. He, Y. Ji, J. Power Sources **185**, 754–758 (2008)
5. L.D. Fan, M.M. Chen, H.J. Zhang, C.Y. Wang, C.X. He, Int. J. Hydrog. Energy **42**, 17544–17551 (2017)
6. Y. Wu, B. Dong, J. Zhang, H.B. Song, C.J. Yan, Int. J. Hydrog. Energy **43**, 12627–12636 (2018)
7. J. Zhang, H.B. Song, R. Xu, C.J. Yan, Y. Wu, Int. J. Hydrog. Energy **43**, 12789–12796 (2018)
8. Y. Wu, J. Zhang, L.Y. Li, J. Wei, J.F. Li, X. Yang, C.J. Yan, C.G. Zhou, B. Zhu, ACS Appl. Energy Mater. **1**, 580–588 (2018)
9. C. Zhao, Q.J. Zhou, T. Zhang, L.W. Qu, X. Yang, T. Wei, Mater. Res. Bull. **113**, 25–30 (2019)
10. R. Xu, Y. Wu, X.Y. Wang, J. Zhang, X. Yang, B. Zhu, Int. J. Hydrog. Energy **42**, 17495–17503 (2017)
11. P.D. Lund, B. Zhu, Y.D. Li, S.N. Yun, A.G. Nasibulin, R. Raza, M. Leskela, M. Ni, Y. Wu, G. Chen, L.D. Fan, J. Kim, S. Basu, T. Kallio, I. Pamuk, ACS Energy Lett. **2**, 2752–2755 (2017)
12. Q.J. Zhou, Y. Gao, F. Wang, D.M. An, Y. Li, Y.L. Zou, Z.P. Li, W.B. Wang, Ceram. Int. **41**, 639–643 (2015)

13. X.Y. Wang, M. Afzal, H. Deng, W.J. Dong, B.Y. Wang, Y.Q. Mi, Z.Y. Xu, W. Zhang, C. Feng, Z.Q. Wang, Y. Wu, B. Zhu, Int. J. Hydrog. Energy **42**, 17552–17558 (2017)
14. J. Zhang, W. Zhang, R. Xu, X.Y. Wang, X. Yang, Y. Wu, Int. J. Hydrog. Energy **42**, 22185–22191 (2017)
15. Y.Y. Liu, Y. Wu, W. Zhang, J. Zhang, B.Y. Wang, C. Xia, M. Afzal, J.J. Li, M. Singh, B. Zhu, Int. J. Hydrog. Energy **42**, 17514–17521 (2017)
16. L. Qiu, T. Ichikawa, A. Hirano, N. Imanishi, Y. Takeda, Solid State Ion. **158**, 55–65 (2003)
17. H. Lv, Y.J. Wu, B. Huang, B.Y. Zhao, K.A. Hu, Solid State Ion. **177**, 901–906 (2006)
18. W. Zhou, R. Ran, Z. Shao, J. Power Sources **192**, 231–246 (2009)
19. J.H. Kim, A. Manthiram, J. Mater. Chem. **A3**, 24195–24210 (2015)
20. Q.J. Zhou, F. Wang, Y. Shen, T.M. He, J. Power Sources **195**, 2174–2181 (2010)
21. S.P. Jiang, J.P. Zhang, X. Zheng, J. Eur. Ceram. Soc. **22**, 361–373 (2002)
22. C.C. Wang, T. Becker, K.F. Chen, L. Zhao, B. Wei, S.P. Jiang, Electrochim. Acta **139**, 173–179 (2014)
23. S. Švarcová, K. Wiik, J. Tolchard, H.J. Bouwmeester, T. Grande, Solid State Ion. **178**, 1787–1791 (2008)
24. E. Bucher, A. Egger, G.B. Caraman, W. Sitte, J. Electrochem. Soc. **155**, B1218–B1224 (2008)
25. Z.G. Yang, G.G. Xia, X.H. Li, J.W. Stevenson, Int. J. Hydrog. Energy **32**, 3648–3654 (2007)
26. Z. Yang, G. Xia, J.W. Stevenson, Electrochem. Solid-State Lett. **8**, A168–A170 (2005)
27. W. Qu, L. Jian, J.M. Hill, D.G. Ivey, J. Power Sources **153**, 114–124 (2006)
28. H. Zhang, Z.L. Zhan, X.B. Liu, J. Power Sources **196**, 8041–8047 (2011)
29. J.H. Xiao, W.Y. Zhang, C.Y. Xiong, B. Chi, J. Pu, L. Jian, Int. J. Hydrog. Energy **41**, 9611–9618 (2016)
30. B. Hua, W.Y. Zhang, J. Wu, J. Pu, B. Chi, L. Jian, J. Power Sources **195**, 7375–7379 (2010)
31. Z.H. Sun, S. Gopalan, U.B. Pal, S.N. Basu, Surf. Coat.Technol. **323**, 49–57 (2017)
32. H.Y. Liu, X.F. Zhu, M.J. Cheng, Y. Cong, W.S. Yang, Chem. Commun. **47**, 2378–2380 (2011)
33. H.Y. Liu, X.F. Zhu, M.J. Cheng, Y. Cong, W.S. Yang, Int. J. Hydrog. Energy **38**, 1052–1057 (2013)
34. Y.Y. Rao, Z.B. Wang, L. Chen, R.F. Wu, R.R. Peng, Y.L. Lu, Int. J. Hydrog. Energy **38**, 14329–14336 (2013)
35. X.J. Liu, D. Han, H. Wu, X. Meng, F.R. Zeng, Z.L. Zhan, Int. J. Hydrog. Energy **38**, 16563–16568 (2013)
36. L. Shao, Q. Wang, L.S. Fan, P.X. Wang, N.Q. Zhang, K.N. Sun, Chem. Commun. **52**, 8615–8618 (2016)
37. S.Y. Zhen, W. Sun, P.Q. Li, G.Z. Tang, D. Rooney, K.N. Sun, X.X. Ma, J. Power Sources **315**, 140–144 (2016)
38. L. Shao, P.X. Wang, Q. Zhang, L.S. Fan, N.Q. Zhang, K.N. Sun, J. Power Sources **343**, 268–274 (2017)
39. Q.J. Zhou, T. Wei, Z.P. Li, D.M. An, X.Q. Tong, Z.H. Ji, W.B. Wang, H. Lu, L.Y. Sun, Z.Y. Zhang, K. Xu, J. Alloys Compd. **627**, 320–323 (2015)
40. Y. Cheng, Q.J. Zhou, W.D. Li, T. Wei, Z.P. Li, D.M. An, X.Q. Tong, Z.H. Ji, X. Han, J. Alloys Compd. **641**, 234–237 (2015)
41. F.M. Ye, Q.J. Zhou, K. Xu, Z.Y. Zhang, X. Han, L. Yang, J. Xu, H.Y. Xu, K.J. Wu, Y.J. Guan, J. Alloys Compd. **680**, 163–168 (2016)
42. X. Yang, J.C. Liu, F.L. Chen, Y.H. Du, A. Deibel, T.M. He, Electrochim. Acta **290**, 440–450 (2018)
43. A. Petric, H. Ling, J. Am. Ceram. Soc. **90**, 1515–1520 (2007)
44. Y. Cheng, Q.J. Zhou, L.B. Chen, Y.T. Xie, Mater. Lett. **193**, 105–107 (2017)
45. F.F. Dong, D.J. Chen, Y.B. Chen, Q. Zhao, Z.P. Shao, J. Mater. Chem. **22**, 15071–15079 (2012)
46. Q.J. Zhou, L.B. Chen, Y. Cheng, Y.T. Xie, Ceram. Int. **42**, 10469–10471 (2016)